Available online at website: https://journal.bcrec.id/index.php/bcrec

Bulletin of Chemical Reaction Engineering & Catalysis, 21 (4) 2026, 825-839

Original Research Article

Hydrothermal Synthesis of Fe-doped Bi_2O_3 Nanoparticles for Rapid Photocatalytic Degradation of Methylene Blue

Kovan Ibrahim Ali*, Jamal A. Abbas

Department of Chemistry, College of Science, University of Duhok, Duhok, Iraq.

Received: 27th May 2026; Revised: 10th August 2026; Accepted: 12th August 2026
Available online: 15th August 2026; Published regularly: December 2026

Abstract

The increasing discharge of organic dyes into aquatic environments requires efficient and sustainable remediation strategies. Although Fe-doped Bi_2O_3 has shown promising photocatalytic performance, the effects of Fe content on its photocatalytic behavior under xenon-lamp irradiation remain insufficiently understood. This study aimed to synthesize different amounts of Fe-doped Bi_2O_3 nanoparticles via a hydrothermal approach and subsequently evaluate their photocatalytic performance toward the degradation of methylene blue (MB). Monoclinic α-Bi_2O_3 was formed as confirmed by X-ray diffraction analysis, without any detectable secondary phases, suggesting that Fe species were either incorporated into the Bi_2O_3 lattice or well dispersed in the matrix. Furthermore, the band gap energy decreased from 2.92 eV to 2.66 eV as determined by diffuse reflectance spectroscopy combined with Tauc analysis. Photoluminescence analysis revealed a decrease in emission intensity, indicating suppressed electron-hole recombination and enhanced photogenerated charge separation. Among the prepared samples, the sample with 10 wt% Fe-doped Bi_2O_3 exhibited the highest photocatalytic activity with about 99% degradation of 10 ppm MB within 14 min at optimum experimental conditions (pH of 8, 45 °C). The degradation followed a pseudo-first-order kinetic model with a rate constant of 0.134 min^{-1}. The improved photocatalytic efficiency is attributed to Fe-induced band-gap narrowing and enhanced charge separation, highlighting its potential for wastewater treatment applications.

Keywords: Fe-doped Bi_2O_3; photocatalytic degradation; methylene blue; xenon-lamp irradiation; charge separation

How to Cite: Ali, K. I., Abbas, J. A. (2026). Hydrothermal Synthesis of Fe-doped Bi_2O_3 Nanoparticles for Rapid Photocatalytic Degradation of Methylene Blue. *Bulletin of Chemical Reaction Engineering & Catalysis*, 21 (4), 825-839. (DOI: 10.9767/bcrec.20754)

Permalink/DOI: https://doi.org/10.9767/bcrec.20754

1. Introduction

Industrial wastewater is often composed of many harmful chemicals, such as heavy metals, dyes, phenolic compounds and metalloids. Many of these chemicals are toxic to the ecosystem and human health, and can persist in the environment for a long time. The conventional methods are not always effective and therefore, the removal of these pollutants by efficient and durable methods is still needed [1-3].

Methylene blue (MB), a common cationic dye, is often used as a model pollutant, because of its chemical stability, toxicity, and resistance to biodegradation. The characteristic absorption peak of MB in an aqueous solution is about 664 nm, which is convenient to monitor the degradation behavior. The semiconductor-based photocatalysis has been widely used for the dye removal, due to its high efficiency and relatively low cost under the light irradiation [4,5]. In addition, Advanced Oxidation Processes (AOPs) have attracted attention due to their ability to generate highly reactive species that can degrade organic pollutants while limiting secondary contamination [6,7]. However, conventional photocatalysts such as TiO_2 and ZnO mainly operate under ultraviolet (UV) light, which

* Corresponding Authors.
Email: Kovan.ali@uod.ac (K.I. Ali)

represents only a small portion of the solar spectrum, thereby limiting their practical applications [7,8]. Bismuth oxide (Bi_2O_3), a p-type semiconductor with several polymorphic forms, has therefore been explored as a visible-light-responsive material because of its relatively narrow band gap (2.1–2.8 eV) and suitable electronic properties. The incorporation of transition-metal ions, particularly Fe^{3+}, introduces defect-related energy levels within the band gap, thereby enhancing visible-light absorption and promoting charge-carrier separation [9,10].

Previous studies have demonstrated that Fe incorporation into Bi_2O_3-based photocatalysts can improve photocatalytic performance through modification of the electronic structure, enhancement of visible-light absorption, and promotion of charge-carrier separation [11-16]. However, despite these successes, there is still a lack of in-depth understanding of the effects of Fe content on photocatalytic kinetics and reaction mechanisms, especially under xenon-lamp irradiation. Furthermore, many Bi_2O_3-based systems fail to achieve rapid and efficient dye degradation within a short irradiation time. In this work, we report the hydrothermal synthesis of Fe-doped α-Bi_2O_3 nanoparticles and a systematic study of their structural, optical and photocatalytic properties. The optimal Fe-doped Bi_2O_3 sample shows rapid degradation, achieving near complete removal of methylene blue within a short irradiation period. The results suggest that Fe doping may change the electronic structure and improve the charge-carrier dynamics, suggesting Fe-doped Bi_2O_3 as a potential photocatalyst for wastewater treatment.

2. Materials and Method

All chemicals used in this study were analytical grade and used without further purification.

2.1. Synthesis of Fe-doped Bi_2O_3 Nanoparticles

Fe-doped Bi_2O_3 nanoparticles with Fe contents of 1, 3, 5, 7, 10, and 13 wt% (expressed as Fe_2O_3 equivalent relative to Bi_2O_3) were synthesized using a hydrothermal method. In a typical synthesis, 0.00386 mol (1.87 g) of bismuth nitrate pentahydrate ($Bi(NO_3)_3.5H_2O$) was dissolved in 80 mL of a 1:1 (v/v) water–ethanol mixture under continuous magnetic stirring. Then Ferric chloride hexahydrate ($FeCl_3 \cdot 6H_2O$) was added in different amounts: 1.13×10^{-4} mol (0.0304 g), 3.37×10^{-4} mol (0.0912 g), 5.63×10^{-4} mol (0.1521 g), 7.88×10^{-4} mol (0.2130 g), 1.12×10^{-3} mol (0.3040 g) and 1.46×10^{-3} mol (0.3950 g) which corresponded to Fe doping concentrations of 1, 3, 5, 7, 10 and 13 wt%, respectively. The mixture was stirred until a clear and homogeneous solution was obtained. The pH was subsequently adjusted to 9 by adding 1 M NaOH gradually with continuous stirring. The obtained suspension was stirred for another 1 h. Then it was transferred to a Teflon-lined stainless steel autoclave for hydrothermal treatment at 180 °C for 12 h. After cooling the solution to room temperature the precipitate was obtained by centrifugation. The material was subsequently rinsed multiple times with deionized water and ethanol to eliminate residual ions and contaminants. The obtained product was then dried overnight at 60 °C. Finally, the dried powders were calcined in air at 500 °C for 2 h to improve crystallinity and obtain the Fe-doped Bi_2O_3 nanoparticles [14-16].

2.2. Characterizations

A variety of analytical techniques were employed to investigate the structural and physicochemical properties of the synthesized nanoparticles. The phase composition and crystal structure were examined using X-ray diffraction (XRD) with a Philips Analytical PW1730 diffractometer (Netherlands) employing Cu-Kα radiation (λ = 1.5406 Å). Surface morphology and particle size were analyzed by field-emission scanning electron microscopy (FESEM, JEOL JSM-7600F, Japan).

Elemental composition and distribution were determined by energy-dispersive X-ray spectroscopy (EDX, Oxford Instruments X-Max detector) operated at an accelerating voltage of 15 kV. Fourier-transform infrared (FTIR) spectra were recorded using a Bruker Tensor 27 spectrometer (Germany) in the 4000–400 cm^{-1} range using the KBr pellet method. The optical absorption properties of the samples were examined by UV–Vis diffuse reflectance spectroscopy (DRS) using a Shimadzu UV-2600 spectrophotometer (Japan) over the wavelength range of 200–1200 nm. Photoluminescence (PL) spectra were obtained using a spectrofluorometer with an excitation wavelength of 320 nm to evaluate charge-carrier recombination behavior.

2.3. Photocatalytic Degradation of Methylene Blue (MB)

Methylene blue was used as a model organic pollutant for the evaluation of the photocatalytic activity of the prepared nanoparticles. In a typical experiment, 0.1 g of Fe-doped Bi_2O_3 catalyst with 10 wt% Fe was added to 50 mL of 10 ppm aqueous solution of MB and the mixture was continuously stirred by a magnetic stirrer. To demonstrate the effect of radiation on the decomposition of M.B., and to overcome the adsorption effect, the suspension was stirred in the darkness for 30 minutes to achieve an adsorption-desorption

equilibrium between the MB molecules and the catalyst surface.

The reaction mixture was then irradiated using a 100 W xenon lamp (6000 K) positioned approximately 15 cm from the reactor. The photocatalytic reaction was carried out under ambient air conditions. At predetermined time intervals, 3 mL aliquots were collected from the suspension and centrifuged to remove the photocatalyst. The absorbance of the clear supernatant was measured at the characteristic wavelength of methylene blue (λ_{max} = 664 nm) using a UV–Vis spectrophotometer. The photocatalytic degradation efficiency (%) was calculated using the following equation:

$$\text{Degradation efficiency (\%)} = (C_o - C_t)/C_o \times 100\% \quad (1)$$

where C_o and C_t denote the dye concentrations before and after irradiation, respectively. All photocatalytic experiments were performed independently in triplicate (n = 3), and the results are expressed as the mean ± standard deviation (SD) [17,18].

3. Results and Discussion

3.1. XRD Results

Figure 1 shows the X-ray diffraction (XRD) patterns of pure α-Bi_2O_3, α-Fe_2O_3, and Fe-doped Bi_2O_3 nanoparticles with 10 wt% Fe. The diffraction pattern of undoped Bi_2O_3 confirmed the formation of the monoclinic α-Bi_2O_3 phase. The characteristic diffraction peaks are consistent with the standard reference data, and no impurity phase was observed within the XRD detection limit [19]. The main diffraction peaks of α-Bi_2O_3 characteristic of Fe-doped Bi_2O_3 are retained, and no additional peaks corresponding to crystalline Fe_2O_3 are present. This suggests that the Fe species are either incorporated in the Bi_2O_3 matrix or are homogenously dispersed in it without the formation of any secondary phases detectable by XRD. The incorporation of iron causes a small shift of the diffraction peaks to higher 2θ values and broadening of the peaks. The observed peak shift and broadening suggest distortion in the Bi_2O_3 crystal lattice after Fe incorporation. This behavior may be related to the substitution of larger Bi^{3+} ions (≈1.03 Å) by smaller Fe^{3+} ions (≈0.65 Å) or to the incorporation of Fe ions into the Bi_2O_3 structure. Such structural modification can slightly reduce the crystallinity of the material. In addition, the peak broadening may indicate the presence of lattice defects and oxygen-vacancy-related disorder. These defects can then affect a material's structure and its optical properties. Similar X-ray diffraction patterns have been reported for Fe-doped Bi_2O_3 systems [20,21]. The X-ray diffraction (XRD) analysis reveals that the monoclinic structure of α-Bi_2O_3 is retained on addition of Fe but shows lattice distortion due to incorporation or dispersion of Fe.

3.2. FESEM Analysis of Fe-Doped Bi_2O_3 Nanoparticles

The surface morphology and particle size distribution of the Fe-doped Bi_2O_3 sample with 10 wt % Fe were studied by field-emission scanning electron microscopy (FESEM). The FESEM image reveals the formation of nanosized particles with a relatively uniform morphology (Figure 2a). Due to the high surface energy and strong particle-particle interactions, particle agglomeration is common in oxide nanoparticles. As shown in FESEM image measurements, the particle size is in the range of 10-40 nm, with a maximum size of about 25 nm, which is further confirmed by the particle size histogram (Figure 2b). The nanosize morphology and size distribution described here are similar to the previous reports of Bi_2O_3 based photocatalyst synthesized through hydrothermal methods [22]. The observed nanoscale dimensions indicate that the incorporation of Fe affects the particle growth dynamics during the hydrothermal synthesis process. The relatively small particle size is expected to increase the specific surface area, which is usually beneficial for photocatalytic performance due to increased surface active sites and promoted adsorption of dye molecules [23].

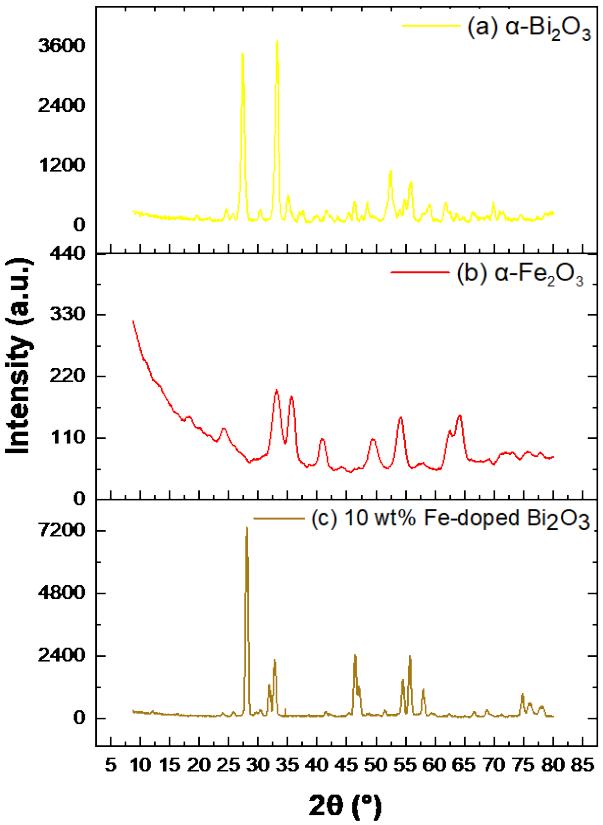

Figure 1. XRD patterns of (a) α-Bi_2O_3, (b) α-Fe_2O_3, and (c) 10 wt% Fe-doped Bi_2O_3.

3.3. Optical Properties

3.3.1. Diffuse Reflectance Spectroscopy (DRS)

Figure 3 shows the diffuse reflectance spectra of pure Bi_2O_3 and Fe-doped Bi_2O_3. Pure Bi_2O_3 shows an absorption edge in the visible region. After Fe doping, the absorption edge shifts toward longer wavelengths (red shift), indicating better visible-light absorption. This behavior is associated with improved photocatalytic performance, together with the smaller band gap and lower PL intensity discussed later.

3.3.2. Band gap (Tauc Plot)

Diffuse reflectance data were analyzed using Kubelka–Munk function, $F(R)=(1-R)^2/(2R)$, where R is the reflectance. The optical band gap energies were determined using the Tauc relation, $(F(R)hv)^n = A(hv-E_g)$, where hv is the photon energy, A is a constant, and n depends on the nature of the electronic transition. In this study, a direct allowed transition was assumed (n = 1/2) for the band gap estimation [24,25]. The direct band gap of the pristine Bi_2O_3 sample is 2.92 eV, and the direct band gap of the Fe-doped Bi_2O_3 sample is reduced to 2.66 eV (Figure 4).

This decrease can be attributed to the Fe-induced modification of the electronic structure of Bi_2O_3. This result agrees with the redshift observed in the DRS spectra. The Tauc analysis reveals that the doping with iron decreases the energy needed for the electronic transition. This modification increases the photocatalytic activity of the material.

3.3.3. Photoluminescence (PL) analysis

The behavior of the recombination of the photogenerated charge carriers was studied by PL spectroscopy. PL emission is caused by the electron–hole recombination and thus can give information about the charge-carrier dynamics in semiconductor materials. When the sample is illuminated, electrons are excited to the conduction band and holes are left behind in the valence band. The photogenerated charge carriers either participate in surface reactions or recombine, which decreases the photocatalytic efficiency [26]. Figure 5 shows the PL spectra of Bi_2O_3 and 10 wt% Fe-doped Bi_2O_3 obtained at an excitation wavelength of 320 nm in the emission region of 330-900 nm. The pure bismuth oxide sample shows a broad emission band in the visible region, which is usually attributed to defect states, whereas the PL intensity of the Fe-doped sample is much lower. This reduction suggests suppressed electron-hole recombination and improved charge separation, likely due to Fe-related defect states acting as charge- trapping sites [27-29].

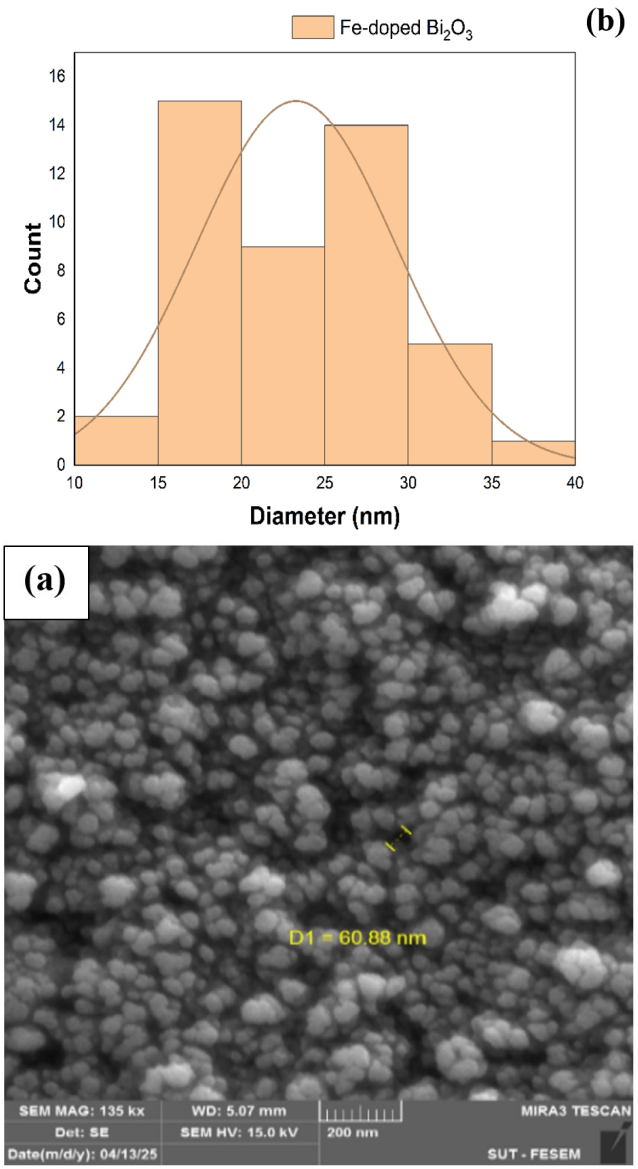

Figure 2. (a) FESEM image and (b) particle-size distribution histogram of 10 wt% Fe-doped Bi_2O_3 nanoparticles.

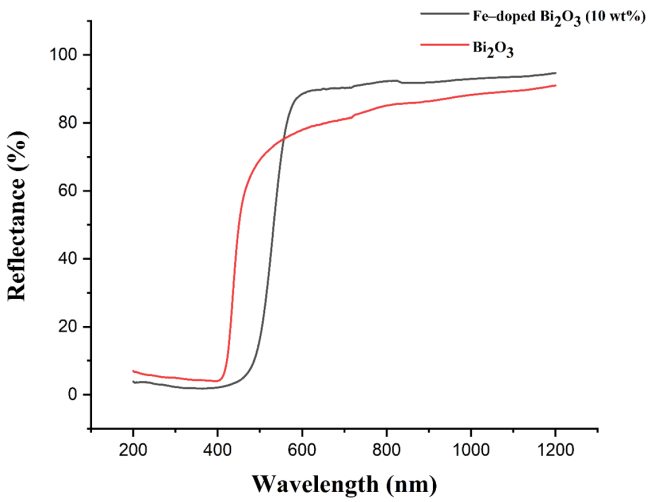

Figure 3. Diffuse reflectance spectra of Bi_2O_3 and Fe-doped Bi_2O_3 (10 wt% Fe), showing a noticeable red shift in the absorption edge for the Fe-doped sample.

3.4. Energy-Dispersive X-ray Spectroscopy (EDX)

The EDX spectrum (Figure 6) shows peaks corresponding to bismuth, oxygen, and iron, with no detectable impurity elements within the sensitivity limits of the technique. Quantitative EDX analysis of the Fe-doped Bi_2O_3 sample showed a composition of about 81.87% bismuth, 10.82% oxygen and 7.31% iron. In view of the semi-quantitative and surface-sensitive nature of EDX, the difference between the measured iron concentration and the intended doping level can be understood. According to the X-ray diffraction (XRD) data, these results suggest that iron is probably incorporated or uniformly distributed in the Bi_2O_3 matrix without the presence of detectable secondary phases. This incorporation may influence the optical properties and promote improved charge-carrier separation [29].

3.5. FTIR Analysis

Figure 7 shows the FTIR spectra of Bi_2O_3, Fe_2O_3 and Fe-doped Bi_2O_3 nanoparticles with 10 wt% Fe. The absorption bands located at approximately 606 cm^{-1} and 497 cm^{-1} in pure Bi_2O_3 are assigned to Bi–O stretching vibrations and Bi–O–Bi lattice modes characteristic of monoclinic α-Bi_2O_3. A weak band near 1380 cm^{-1} may originate from residual precursor species or adsorbed surface groups.

For the Fe-doped Bi_2O_3 sample, the Bi–O-related vibrational bands shifted slightly toward lower wavenumbers (approximately 597 cm^{-1} and 489 cm^{-1}) together with minor peak broadening. These changes indicate alterations in the local metal–oxygen bonding environment and possible lattice distortion after Fe incorporation into the Bi_2O_3 structure. In addition, a weak shoulder in the 630–680 cm^{-1} region may be related to Fe-

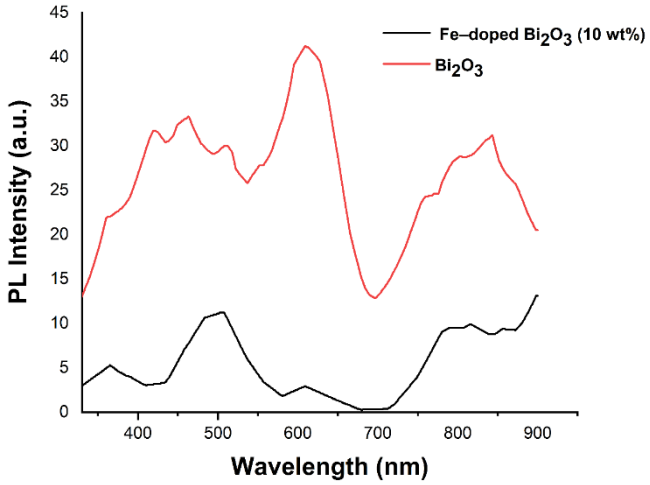

Figure 5. Photoluminescence (PL) spectra of Bi_2O_3 and 10 wt% Fe-doped Bi_2O_3 nanoparticles.

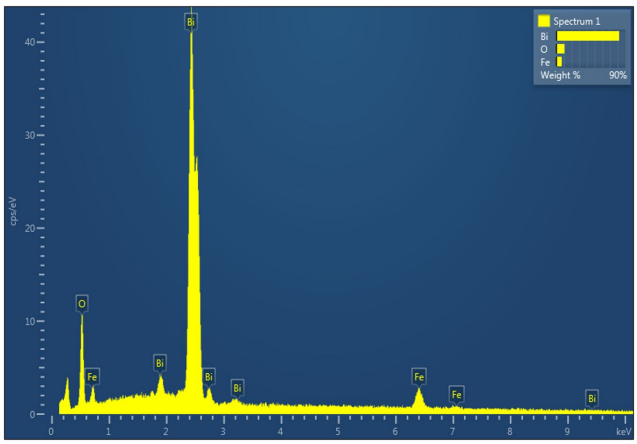

Figure 6. EDX spectrum of 10 wt% Fe-doped Bi_2O_3 nanoparticles.

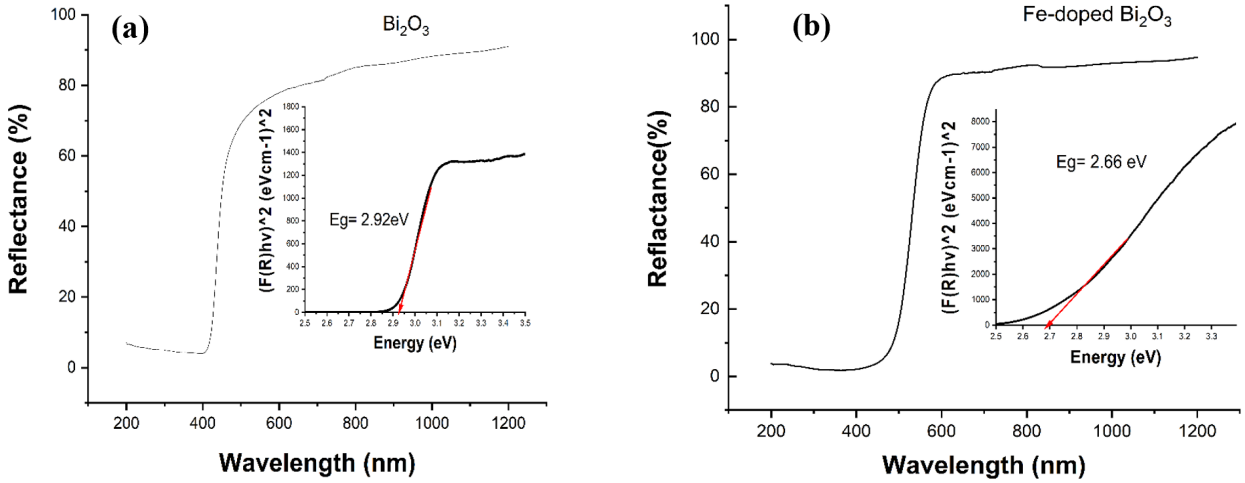

Figure 4. Comparative Tauc plots for (a) direct band-gap determination of Bi_2O_3 and (b) Fe-doped Bi_2O_3, showing a narrowing of the band gap after Fe doping.

associated lattice vibrations or defect-induced structural disorder. However, this assignment remains tentative because of overlap with Bi–O vibrational bands in the low-wavenumber region. No additional distinct Fe_2O_3 absorption bands were detected in the Fe-doped Bi_2O_3 spectrum, suggesting that iron oxide did not form a clearly separated secondary crystalline phase, in agreement with the XRD analysis. Overall, the observed band shifts and peak broadening indicate local structural modifications and changes in the metal–oxygen bonding environment after Fe doping. These structural modifications may influence the optical and photocatalytic properties of Fe-doped Bi_2O_3, together with the reduced band gap and lower PL intensity discussed in the previous sections [30,31].

3.6. Photocatalytic Degradation of Methylene Blue (MB)

3.6.1. Dark adsorption test

Before light irradiation, the catalyst suspension containing methylene blue was stirred in the dark for 30 min to reach adsorption–desorption equilibrium. As shown in Figure 8, only a slight decrease in the absorbance of methylene blue at approximately 664 nm was observed after this dark period. This indicates that adsorption of MB on the Fe-doped Bi_2O_3 surface is minimal, confirming that the subsequent dye removal under xenon-lamp irradiation is mainly attributed to photocatalytic degradation.

3.6.2. Photolysis test

A control photolysis experiment was performed under the same xenon-lamp irradiation conditions, but without a photocatalyst. Figure 9 shows a slight decrease in the absorbance of methylene blue at about 664 nm upon irradiation. The experiment was carried out under uniform irradiation of a xenon lamp without a photocatalyst. The data indicate that the direct photolysis of methylene blue (MB) is not significant under the experimental conditions. The rapid degradation of dye in the presence of Fe-doped Bi_2O_3 is mainly due to its photocatalytic nature.

3.6.3. Effect of Fe content

The photocatalytic performance of Fe-doped Bi_2O_3 nanoparticles, which incorporated different amounts of iron (1–13 wt%), was evaluated by observing the degradation of methylene blue (10 ppm) under xenon-lamp irradiation. The Fe-doped Bi_2O_3 exhibited higher photocatalytic activity compared to pure Bi_2O_3. This fact highlights that the incorporation of iron improves the photocatalytic properties of the material. Figure 10 shows that the normalized concentration (C_t/C_0) decreased with the increase in Fe content and reached the minimum value at 10 wt%, indicating a gradual enhancement of the photocatalytic activity up to this composition. Under these conditions, the 10 wt% Fe-doped Bi_2O_3 sample was able to attain almost complete degradation in 14 min. In contrast, further increasing the iron content to 13 wt% resulted in a slight decline in photocatalytic activity.

The observed decrease can be explained by the creation of an excessive number of defect sites caused by the dopant. However, these imperfections may act as recombination sites for the electron-hole pairs generated by the light, and thus reduce the charge separation efficiency. In addition, the enhanced dopant concentration may limit the number of active surface sites, leading to poor light absorption and subsequent reduction of

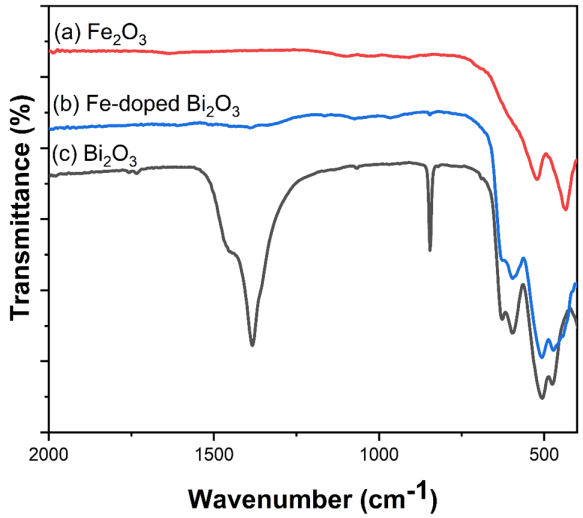

Figure 7. FTIR spectra of (a) Fe_2O_3, (b) 10 wt % Fe-doped Bi_2O_3, and (c) Bi_2O_3 nanoparticles.

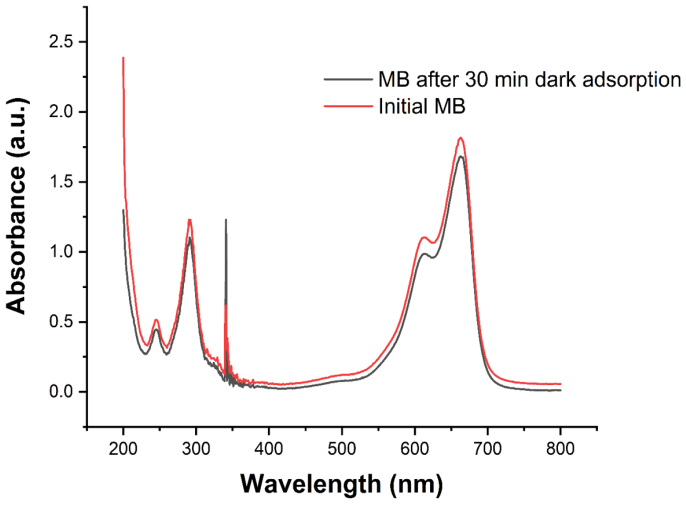

Figure 8. UV–Vis absorption spectra of methylene blue before and after 30 min of dark adsorption.

the photocatalytic activity. These observations are in line with previous studies on transition metal doped Bi_2O_3 systems, which revealed that a certain amount of dopant increases activity and excess doping deteriorates the performance [32].

3.6.4. Effect of pH

The pH of the solution plays an important role in the photocatalytic degradation process which affects the surface charge of the catalyst, the adsorption behavior of dye molecules and the generation of reactive oxygen species. Figure 11 shows the influence of pH on the degradation efficiency of the 10 wt% Fe-doped Bi_2O_3 catalyst. The highest degradation efficiency was obtained at pH of 8, whereas the efficiencies were lower under strongly acidic and highly alkaline conditions. In aqueous solution, methylene blue carries a net positive charge, and the electrostatic attraction between the negatively charged catalyst surface and the dye molecules is increased under slightly alkaline conditions, thereby improving adsorption and photocatalytic efficiency. In addition, the higher concentration of OH^- ions under slightly alkaline conditions promotes the formation of hydroxyl radicals (•OH) through reactions with photogenerated holes, thereby enhancing the photocatalytic degradation process. However, at higher or lower pH values, the adsorption efficiency is decreased, and charge transfer mechanisms are hindered. Under highly alkaline conditions, an excess of OH^- may also compete with dye molecules for active sites, resulting in lower photocatalytic degradation efficiency. This pH-dependent behavior is consistent with previous studies of dye degradation using semiconductor photocatalysts that have shown that surface charge interactions influence both adsorption and degradation efficiency through the generation of reactive oxygen species [33-35].

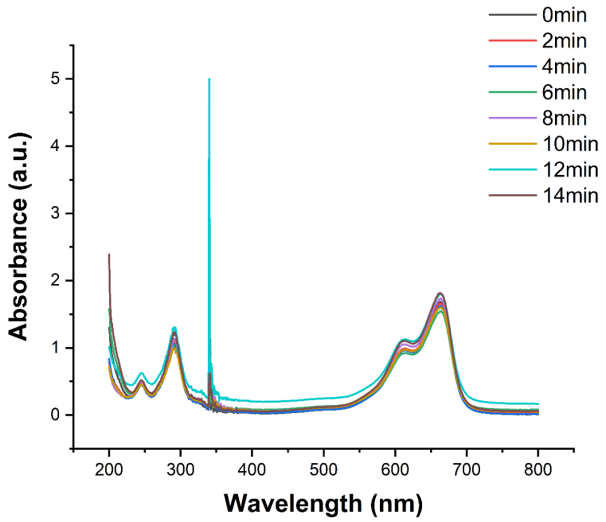

Figure 9. UV–Vis absorption spectra of methylene blue solution under xenon-lamp irradiation in the absence of photocatalyst (photolysis control).

3.6.5. Effect of catalyst dosage

The effect of catalyst dosage on photocatalytic degradation was studied by changing the catalyst amount from 0.025 to 0.1 g while keeping the same MB concentration (10 ppm), solution volume (50 mL) and other experimental conditions unchanged (Figure 12). Increasing the catalyst dosage enhanced the degradation efficiency because of the greater availability of active surface sites and increased

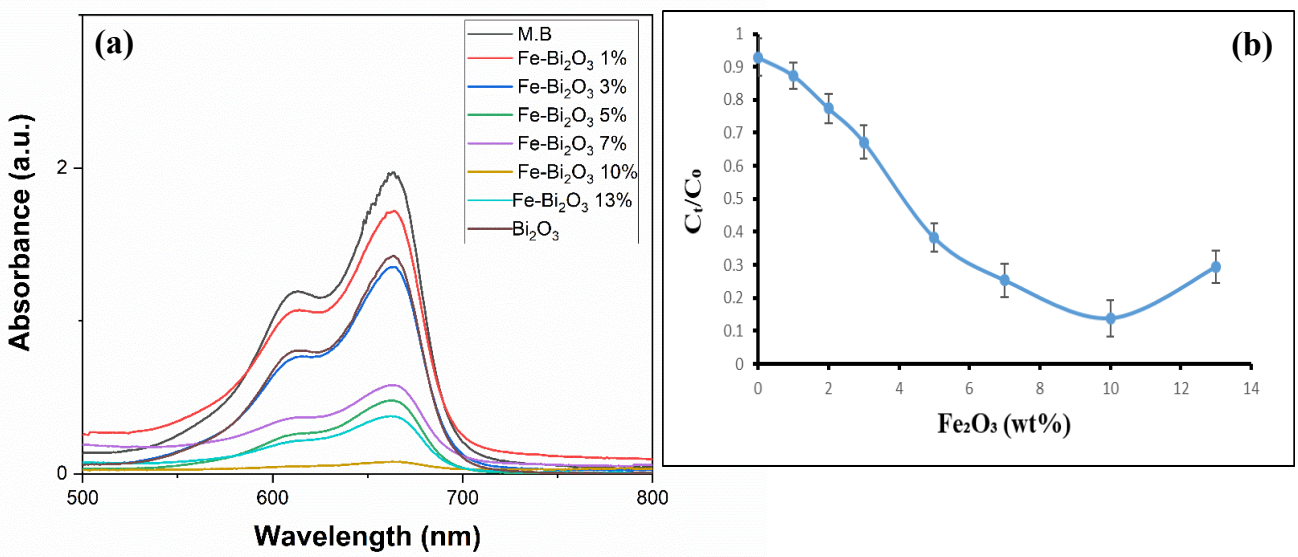

Figure 10. (a) UV–Vis spectra of MB degradation using Fe-doped Bi_2O_3 (1–13 wt% Fe), and (b) C_t/C_0 variation showing the effect of Fe content on photocatalytic performance. Error bars represent the standard deviation (SD) of three independent experiments (n = 3).

light harvesting within the reaction system. The highest photocatalytic activity was achieved at a catalyst dosage of 0.1 g, and therefore this loading was selected for the subsequent photocatalytic experiments under the present conditions. At higher catalyst loadings, excessive particle agglomeration and increased light scattering can reduce effective light penetration into the reaction medium, thereby limiting photocatalytic efficiency. Similar trends have been reported in various photocatalytic systems with different catalyst compositions [36].

3.6.6. Effect of temperature

The effect of temperature on the photocatalytic degradation of methylene blue (MB) was investigated within the temperature range of 25–55 °C under otherwise identical experimental conditions (Figure 13). The degradation efficiency increased gradually with the increase of temperature from 25 °C to 45 °C, which indicated that moderately elevated temperature promotes photocatalytic degradation. Maximum degradation efficiency was obtained at 45 °C. Further increase in temperature to 55 °C resulted in a slight decrease in the photocatalytic performance. The moderate increase in temperature also facilitates the diffusion of methylene blue molecules to the catalyst surface, thereby increasing the frequency of effective collisions with the active sites and accelerating the photocatalytic

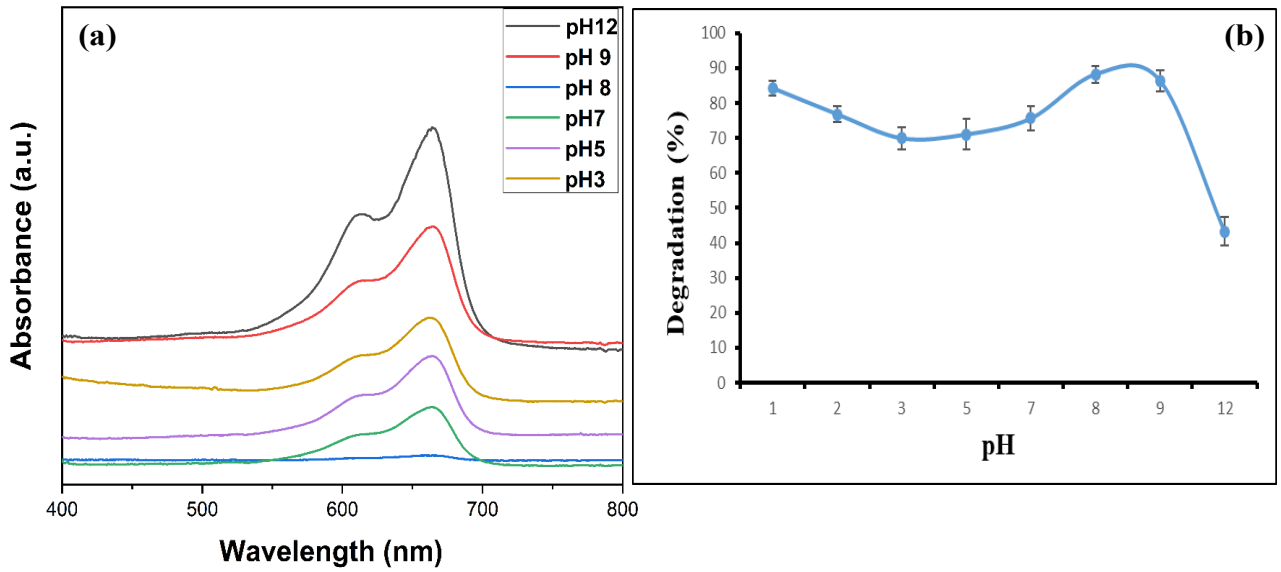

Figure 11. (a) UV–Vis absorption spectra showing the effect of pH on MB degradation, and (b) corresponding degradation efficiency of MB (10 ppm) under xenon-lamp irradiation using 10 wt% Fe-doped Bi_2O_3 at 45 °C. Error bars represent the standard deviation (SD) of three independent experiments (n = 3).

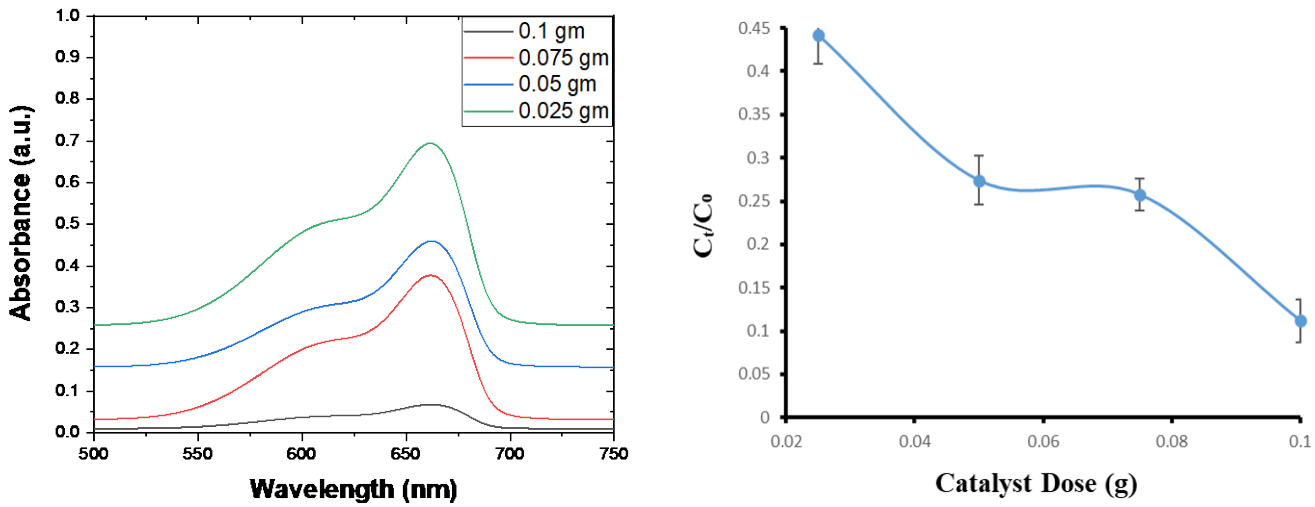

Figure 12. (a) UV–Vis spectra and (b) C_t/C_0 values for MB degradation at different catalyst dosages. Error bars represent the standard deviation (SD) of three independent experiments (n = 3).

degradation reaction. The improved degradation efficiency up to 45 °C is ascribed to the enhanced reaction kinetics, mass transfer, and dye molecule-catalyst surface interactions. However, very high temperatures have a detrimental impact on the photocatalytic process owing to the lower availability of dissolved oxygen, higher recombination of photogenerated electron-hole pairs, and weaker adsorption of dye molecules onto the catalyst surface. The reduced dissolved oxygen concentration at elevated temperatures limits the generation of reactive oxygen species (ROS), thereby decreasing the photocatalytic degradation efficiency. Similar temperature-dependent behavior was reported in previous studies on the photocatalytic degradation of organic dyes, where a moderate increase in temperature is beneficial for the photocatalytic reaction rates, while excessively high temperatures might be detrimental to the generation of reactive oxygen species and promote the recombination of charge carriers [37, 38].

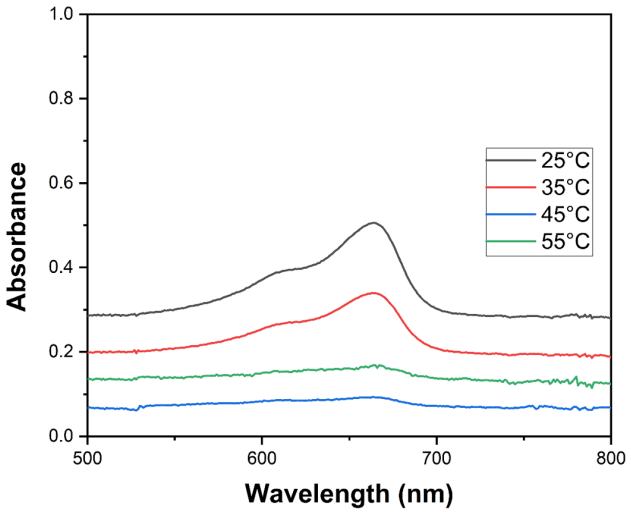

Figure 13. Effect of reaction temperature on the photocatalytic degradation of methylene blue using 10 wt% Fe-doped Bi_2O_3 under xenon-lamp irradiation.

3.6.7. Effect of irradiation time

The effect of irradiation time on the degradation of methylene blue (MB) was investigated under optimized conditions (0.1 g catalyst, pH of 8, 45 °C), as shown in Figure 14. With the increase of irradiation time, the degradation efficiency increased, suggesting that the photocatalytic activity remained stable under xenon lamp irradiation. The degradation was rapid at the beginning, and almost complete degradation was achieved within 14 minutes. Under such conditions, about 99% of MB was degraded, indicating the high photocatalytic activity of 10 wt% Fe-doped Bi_2O_3 catalyst.

The present results demonstrate that the primary objective of improving the visible-light photocatalytic performance of Bi_2O_3 through Fe incorporation was successfully achieved. The enhanced photocatalytic performance of the optimized 10 wt% Fe-doped Bi_2O_3 photocatalyst can be attributed to the combined structural, morphological, and optical modifications introduced by Fe incorporation. XRD, EDX, and FTIR analyses indicated the incorporation or homogeneous dispersion of Fe species within the Bi_2O_3 matrix, accompanied by lattice distortion and modification of the metal–oxygen bonding

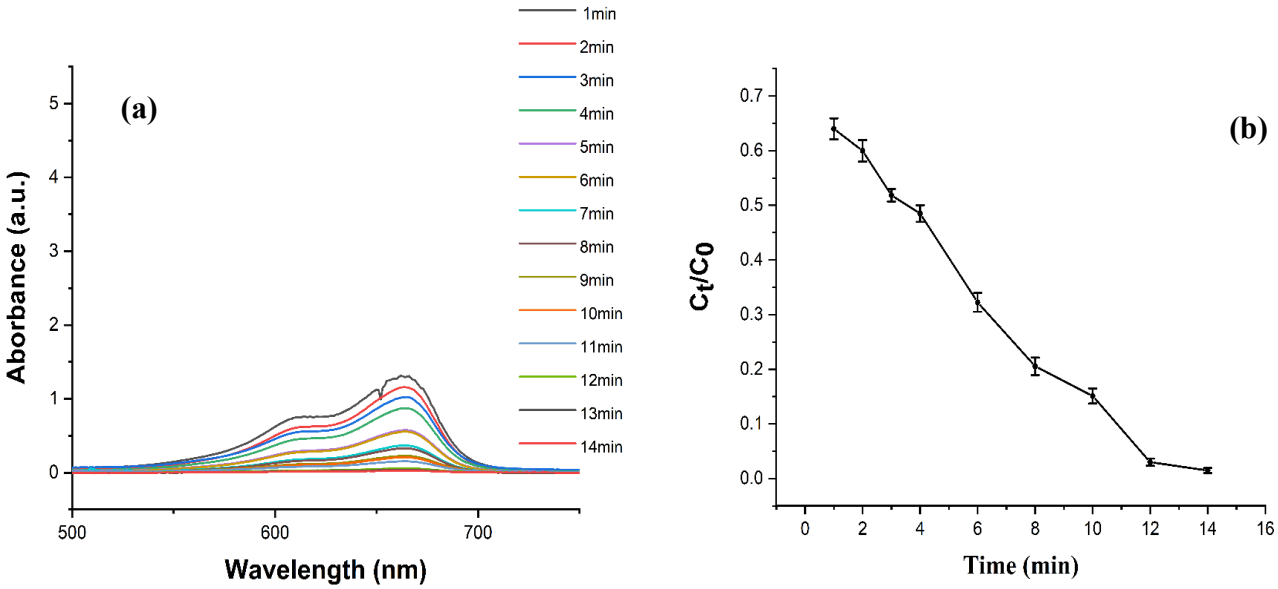

Figure 14. (a) UV–Vis spectra of methylene blue (10 ppm, pH of 8, 45 °C) under Xenon-lamp irradiation (100 W), and (b) degradation profile (C_t/C_0 vs. time) for 10 wt% Fe-doped Bi_2O_3 catalyst. Error bars represent the standard deviation (SD) of three independent experiments (n = 3).

environment. These structural modifications may introduce defect-related trapping sites that influence charge-carrier behavior. The nanosized morphology observed by FESEM may provide abundant surface-active sites for photocatalytic reactions. Furthermore, the red shift in the absorption edge and the reduction in the optical band gap from 2.92 to 2.66 eV enhanced visible-light absorption. Moreover, the lower PL intensity suggests suppressed electron–hole recombination and improved charge separation. Consequently, the superior photocatalytic activity of the optimized 10 wt% Fe-doped Bi_2O_3 sample is attributed to the combined effects of enhanced visible-light absorption, reduced charge-carrier recombination, defect-mediated charge trapping, and the availability of nanoscale surface-active sites. In contrast, the slight decrease in activity at 13 wt% Fe may result from excessive defect sites that act as recombination centers and reduce the availability of photocatalytically active surface sites [9,21]. These findings are consistent with previous reports on Fe-modified Bi_2O_3 photocatalysts, while a detailed comparison with previously published studies is presented in Section 3.10 and Table 1.

To further demonstrate the enhancement in photocatalytic performance resulting from Fe incorporation, the photocatalytic activity of the optimized 10 wt% Fe-doped Bi_2O_3 was directly compared with that of pure Bi_2O_3 under identical experimental conditions (Figure 15). The 10 wt% Fe-doped Bi_2O_3 exhibited a substantially higher MB degradation efficiency after 14 min (approximately 99%) than pure Bi_2O_3 (approximately 27%), further demonstrating the enhanced photocatalytic performance following Fe incorporation.

3.7. Kinetic study

The photocatalytic degradation kinetics were analyzed using the pseudo-first-order model based on the Langmuir–Hinshelwood approach:

$$\ln (C_0/C_t) = kt \quad (2)$$

where C_0 and C_t represent the initial and time-dependent concentrations of methylene blue, respectively, k is the apparent rate constant, and t is the irradiation time. The kinetic analysis was carried out using the initial linear region (0–4 min) of the $\ln(C_0/C_t)$ versus irradiation time plot (Figure 16), where a strong linear relationship was obtained (R^2 = 0.9958). Non-linear behavior was observed at longer irradiation times and was attributed to lower dye concentration, surface saturation effects, and limitations in mass transfer. Hence, the kinetic analysis was limited to the initial linear part. The apparent rate constant (k) for the optimized 10 wt% Fe-doped Bi_2O_3 photocatalyst was found to be 0.134 min^{-1}. This indicates a high degradation rate and fast photocatalytic degradation at the given conditions. The apparent rate constant of 0.134 min^{-1} confirms the rapid initial degradation of MB under the optimized experimental conditions. This finding is in agreement with the previous research on semiconductor photocatalysts [39 40]. To evaluate the photocatalytic capabilities more thoroughly, the activity of the Fe-doped α-Bi_2O_3 photocatalyst was compared with that of typical Fe-doped Bi_2O_3 systems reported in the current body of research. The comparison was based primarily on the apparent rate constant, which is considered a more reliable parameter in evaluating the photocatalytic performance than degradation efficiency alone.

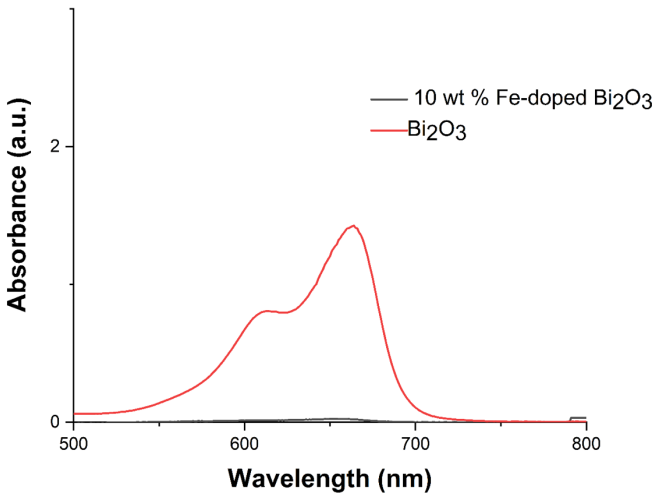

Figure 15. Comparison of the UV–Vis absorption spectra of methylene blue after photocatalytic treatment with pure Bi_2O_3 and 10 wt% Fe-doped Bi_2O_3 under identical experimental conditions.

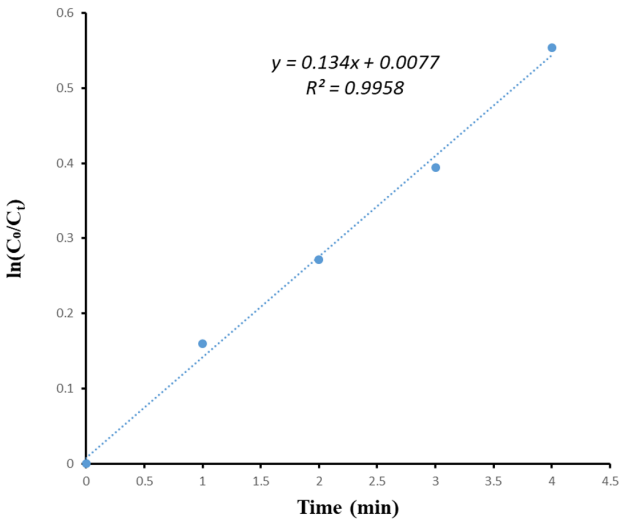

Figure 16. Pseudo-first-order kinetic plot ($\ln(C_0/C_t)$ versus time) for MB degradation over 10 wt% Fe-doped Bi_2O_3 photocatalyst.

The comparison of photocatalytic performance between different studies should be taken with caution as experimental conditions (light source, type of pollutant, catalyst composition and reaction conditions) may differ significantly. Nevertheless, the Fe-doped Bi_2O_3 system reported here can reach a relatively fast degradation rate.

3.8. Reusability of Fe-doped Bi_2O_3 Photocatalyst

The reusability of the Fe-doped Bi_2O_3 photocatalyst was tested for three consecutive degradation cycles, under the same experimental conditions. As shown in Figure 17, the results show a slight decrease in degradation efficiency from 98.7% in the first cycle to 93.8% in the third cycle. The slight decrease in activity could be ascribed to the loss of a small amount of catalyst during recovery or the partial coverage of the surface by reaction intermediates that can block the active sites and reduce the catalytic activity as widely reported for reusable semiconductor photocatalysts [41,42]. Nevertheless, the catalyst retained high photocatalytic activity after repeated reuse, which demonstrated good stability and reusability.

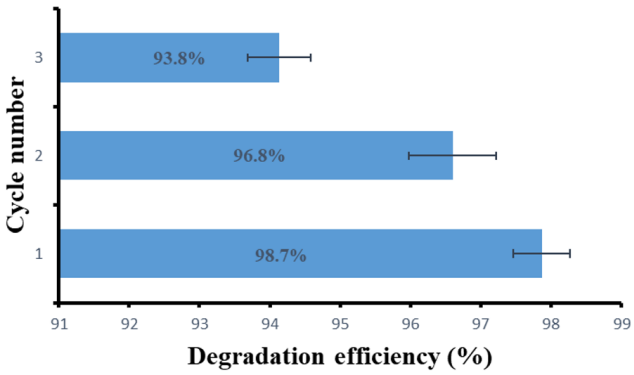

Figure 17. Reusability of the photocatalyst (10 wt% Fe-doped Bi_2O_3) for MB degradation over three consecutive cycles.

3.9. Scavenger Experiments and Mechanistic Study

The photocatalytic mechanism and the main reactive species for the degradation of methylene blue (MB) were studied by scavenger experiments under optimized conditions. Without the addition of scavengers, MB was almost completely degraded (~99%) within 14 min. As shown in Figure 18, the degradation efficiency was decreased to about 60% with the addition of KI (h^+ scavenger), indicating the involvement of the photogenerated holes in the photocatalytic process. The presence of ethanol (•OH scavenger) resulted in a moderate inhibition, with the degradation efficiency decreasing to about 45%, which indicates that the hydroxyl radicals are also important in the degradation reaction. However, the addition of ascorbic acid ($•O_2^-$ scavenger) exhibited the most significant inhibition on photocatalytic activity with the degradation efficiency decreased to about 20%, indicating that the superoxide radicals are the dominant reactive species for MB degradation. The corresponding inhibition percentages

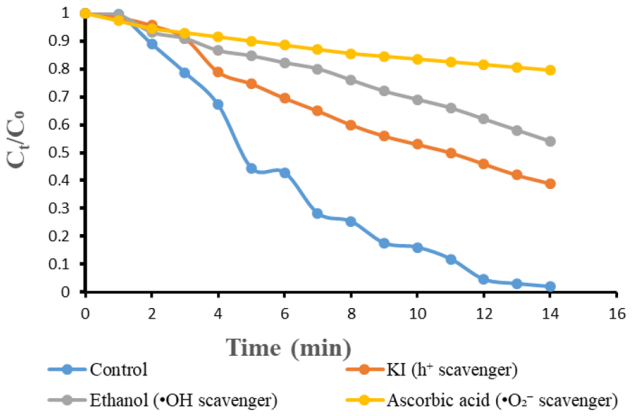

Figure 18. Photocatalytic degradation profiles (C_t/C_0 vs time) of methylene blue (10 ppm) over 10 wt% Fe-doped Bi_2O_3 under xenon-lamp irradiation in the absence and presence of different scavengers (KI, ethanol, and ascorbic acid).

Table 1. Comparison of photocatalytic performance of Fe-doped Bi_2O_3 systems.

Catalyst	Light source	Pollutant	Conditions	Degradation Efficiency (%)	Time min	Rate constant (min^{-1})	References
Fe-doped Bi_2O_3 nanorods (0.5%)	Visible light	Methylene blue	pH ≈ 12, hydrothermal synthesis	93.37	120	---------	[23]
Fe-doped Bi_2O_3	UV light	Amoxicillin	0.02 g catalyst, 50 mL, 10 ppm	76.34	180	0.0079	[12]
Bi_2O_3/Fe (3%)	UV-C + ultrasound	Basic Brown 1 dye	3 g/L catalyst + oxidant	99	180	---------	[16]
Fe-doped Bi_2O_3 nanoparticles (10 wt%)	Xe lamp	Methylene blue	pH of 8, 0.1 g, 45 °C	99	14	0.134	Present work

relative to the control experiment were approximately 39%, 55%, and 80% for KI, ethanol, and ascorbic acid, respectively, indicating that the relative contributions of the reactive species followed the order $\bullet O_2^- > \bullet OH > h^+$.

Radical scavenger experiments are widely used to identify the reactive species involved in photocatalytic processes, including holes (h^+), hydroxyl radicals ($\bullet OH$), and superoxide radicals ($\bullet O_2^-$) [43-45]. The present results are consistent with previous studies on Fe-modified Bi_2O_3 photocatalytic systems, where improved charge separation promotes the generation of reactive oxygen species that contribute to dye degradation [46].

3.10. Comparison with Previous Studies

As shown in Table 1, the present Fe-doped Bi_2O_3 photocatalyst achieved approximately 99% MB degradation within 14 min under xenon-lamp irradiation, showing a shorter degradation time than the selected Fe-doped Bi_2O_3 systems reported in previous studies under their respective experimental conditions.

4. Conclusion

The hydrothermal method was successfully used to synthesize Fe-doped Bi_2O_3 nanoparticles, which show enhanced photocatalytic activity for degradation of methylene blue under irradiation of a xenon lamp. Structural and optical characterizations showed that Fe incorporation reduced the optical band gap from 2.92 eV to 2.66 eV and improved visible light absorption, while the decreased PL intensity suggested suppressed electron- hole recombination and improved charge separation. The optimized Fe-doped Bi_2O_3 sample shows fast degradation with high efficiency following pseudo-first-order kinetics. The scavenger experiments show that superoxide radicals ($\bullet O_2^-$) are the dominant reactive species, while hydroxyl radicals and photogenerated holes also participate in the degradation process. The improved degradation performance can be attributed to the combined effects of enhanced visible-light absorption, possible defect-mediated charge trapping, and improved charge separation.

Acknowledgment

The authors gratefully acknowledge the Department of Chemistry, College of Science, University of Duhok, for providing laboratory facilities and technical support to carry out this research. The authors also express their sincere appreciation to Dr. Rayan Basheer for his assistance with instrumental measurements during this work.

CRedit Author Statement

Author Contributions: Kovan Ibrahim Ali: Conceptualization, Methodology, Investigation, Formal analysis, Data curation, Visualization, Writing original draft preparation. Dr. Jamal A. Abbas: Supervision, Validation, Formal analysis, Writing – review & editing. All authors have read and agreed to the published version of the manuscript. All authors have read and agreed to the published version of the manuscript.

Declaration of Generative AI and AI-assisted Technologies in the Writing

During the preparation of this manuscript, AI-assisted tools were used only for lan-guage improvement and grammar correction. The authors carefully reviewed and edit-ed the manuscript and take full responsibility for the content of the publication.

References

[1] Ahmed, M., Mavukkandy, M.O., Giwa, A., Elektorowicz, M., Katsou, E., Khelifi, O., Naddeo, V., Hasan, S.W. (2022). Recent developments in hazardous pollutants removal from wastewater and water reuse within a circular economy. *NPJ Clean Water*, 5(1), 12. DOI: 10.1038/s41545-022-00154-5.

[2] Al-Sakkaf, M.K., Basfer, I., Iddrisu, M., Bahadi, S.A., Nasser, M.S., Abussaud, B., Drmosh, Q.A., Onaizi, S.A. (2023). An up-to-date review on the remediation of dyes and phenolic compounds from wastewaters using enzymes immobilized on emerging and nanostructured materials: Promises and challenges. *Nanomaterials*, 13(15), 2152. DOI: 10.3390/nano13152152.

[3] Elgarahy, A.M., Elwakeel, K.Z., Mohammad, S.H., Elshoubaky, G. (2021). A critical review of biosorption of dyes, heavy metals and metalloids from wastewater as an efficient and green process. *Cleaner Engineering and Technology*, 4, 100209. DOI: 10.1016/j.clet.2021.100209.

[4] Khan, I., Saeed, K., Zekker, I., Zhang, B., Hendi, A.H., Ahmad, A., Ahmad, S., Zada, N., Ahmad, H., Shah, L.A. (2022). Review on methylene blue: its properties, uses, toxicity and photodegradation. *Water*, 14(2), 242. DOI: 10.3390/w14020242.

[5] Radoor, S., Karayil, J., Jayakumar, A., Parameswaranpillai, J., Siengchin, S. (2021). Release of toxic methylene blue from water by mesoporous silicalite-1: characterization, kinetics and isotherm studies. *Applied Water Science*, 11(7), 110. DOI: 10.1007/s13201-021-01435-z.

[6] Ma, D., Yi, H., Lai, C., Liu, X., Huo, X., An, Z., Li, L., Fu, Y., Li, B., Zhang, M. (2021). Critical review of advanced oxidation processes in organic wastewater treatment. *Chemosphere*, 275, 130104. DOI: 10.1016/j.chemosphere.2021.130104.

[7] Hübner, U., Spahr, S., Lutze, H., Wieland, A., Rüting, S., Gernjak, W., Wenk, J. (2024). Advanced oxidation processes for water and wastewater treatment–Guidance for systematic future research. *Heliyon*, 10(9). DOI: 10.1016/j.heliyon.2024.e30402.

[8] Kamble, G.S., Natarajan, T.S., Patil, S.S., Thomas, M., Chougale, R.K., Sanadi, P.D., Siddharth, U.S., Ling, Y.-C. (2023). BiVO4 as a sustainable and emerging photocatalyst: Synthesis methodologies, engineering properties, and its volatile organic compounds degradation efficiency. *Nanomaterials*, 13(9), 1528. DOI: 10.3390/nano13091528.

[9] Zhang, X., Han, L., Wu, D. (2019). Synthesis, characterization and photocatalytic activity of Fe-doped Bi2O3 nanoparticles. Optoelectronics and *Advanced Materials-Rapid Communications*, 13(9-10), 560-564.

[10] Khan, A.u.R., Ramzan, M., Alanazi, S.J., Al-Mohaimeed, A.M., Ali, S., Imran, M., Majid, M.A., Sarfraz, M.H. (2024). Structural, optical, electrical and photocatalytic investigation of n-type Zn2+-doped α-Bi2O3 nanoparticles for optoelectronics applications. *ACS Omega*, 9(21), 22650-22659. DOI: 10.1021/acsomega.4c02118.

[11] Liang, J., Zhu, G., Liu, P., Luo, X., Tan, C., Jin, L., Zhou, J. (2014). Synthesis and characterization of Fe-doped ß-Bi2O3 porous microspheres with enhanced visible light photocatalytic activity. *Superlattices and Microstructures*, 72, 272-282. DOI: 10.1016/j.spmi.2014.05.005.

[12] Utami, B.A., Sutanto, H., Alkian, I., Sa'Adah, F., Hidayanto, E. (2022). Efficient degradation of amoxicillin using Bi2O3/Fe synthesized by microwave-assisted precipitation method. *Cogent Engineering*, 9(1), 2119534. DOI: 10.1080/23311916.2022.2119534.

[13] Mane, V., Dake, D., Raskar, N., Sonpir, R., Stathatos, E., Dole, B. (2024). Growth in defects and surface area for the photocatalytic performance of GO-based Fe-doped bismuth oxide mesoporous nanocomposite. *Ceramics International*, 50(7), 11179-11189. DOI: 10.1016/j.ceramint.2024.01.019.

[14] Ruiz-Castillo, A.L., Hinojosa-Reyes, M., Camposeco, R., Hinojosa-Reyes, L. (2025). Advances in Bi2O3-based photocatalysts: A review on synergistic modifications and wastewater treatment applications. *Inorganic Chemistry Communications*, 115730. DOI: 10.1016/j.inoche.2025.115730.

[15] Mane, V.A., Dake, D.V., Raskar, N.D., Sonpir, R.B., Chavan, K.M., Gattu, K.P., Stathatos, E., Dole, B.N. (2025). Multifunctional Fe-Doped Bi2O3/TiO2 heterojunctions for environmental remediation and gas sensing. *Surfaces and Interfaces*, 58, 105908. DOI: 10.1016/j.surfin.2025.105908.

[16] Dinesh, G.K., Anandan, S., Sivasankar, T. (2016). Synthesis of Fe-doped Bi2O3 nanocatalyst and its sonophotocatalytic activity on synthetic dye and real textile wastewater. *Environmental Science and Pollution Research*, 23(20), 20100-20110. DOI: 10.1007/s11356-016-7216-8.

[17] Adeleye, A.T., John, K.I., Ighalo, J.O., Ogunniyi, S., Adeyanju, C.A., Adeniyi, A.G., Elawad, M., Omorogie, M.O. (2022). Photocatalytic remediation of methylene blue using hydrothermally synthesized H-Titania and Na-Titania nanotubes. *Heliyon*, 8(12). DOI: 10.1016/j.heliyon.2022.e12610.

[18] Shakoor, M.H., Shakoor, M.B., Jilani, A., Ahmed, T., Rizwan, M., Dustgeer, M.R., Iqbal, J., Zahid, M., Yong, J.W.H. (2024). Enhancing the photocatalytic degradation of methylene blue with graphene oxide-encapsulated g-C3N4/ZnO ternary composites. *ACS Omega*, 9(14), 16187. DOI: 10.1021/acsomega.3c10175.

[19] Senthamilselvi, R., Velavan, R. (2020). Microstructure and photocatalytic properties of bismuth oxide (Bi2O3) nanocrystallites. *Malaya Journal of Matematik*, 5(2), 4870-4874. DOI: 10.26637/MJM0S20/1260.

[20] Zhang, S., Yu, H., Wang, Y., Yan, Y., Dai, J., Shu, D., Wu, X. (2023). Surface Dual Metal Occupations in Fe-Doped Fe x Bi2-x O3 Induce Highly Efficient Photocatalytic CO2 Reduction. *ACS Applied Materials & Interfaces*, 15(20), 25049-25057. DOI: 10.1021/acsami.3c01908.

[21] Dai, Y., Yin, L. (2013). Low Fe-doped Bi2O3 photocatalyst with long wavelength response: crystalline transition and mechanisms by first-principles calculation. *Journal of Alloys and Compounds*, 563, 80-84. DOI: 10.1016/j.jallcom.2013.02.038.

[22] Abu-Dief, A.M., Mohamed, W. (2017). α-Bi2O3 nanorods: synthesis, characterization and UV-photocatalytic activity. *Materials Research Express*, 4(3), 035039. DOI: 10.1088/2053-1591/aa6712.

[23] Mane, V., Dake, D., Raskar, N., Sonpir, R., Stathatos, E., Dole, B. (2023). Magneto-optical properties of Fe-doped bismuth oxide nanorods for photocatalytic and antimicrobial applications. *Results in Chemistry*, 6, 101083. DOI: 10.1016/j.rechem.2023.101083.

[24] Hu, J., Li, H., Huang, C., Liu, M., Qiu, X. (2013). Enhanced photocatalytic activity of Bi2O3 under visible light irradiation by Cu (II) clusters modification. *Applied Catalysis B: Environmental*, 142, 598-603. DOI: 10.1016/j.apcatb.2013.05.079.

[25] Soitah, T.N., Yang, C. (2010). Effect of Fe3+ doping on structural, optical and electrical properties δ-Bi2O3 thin films. *Current Applied Physics*, 10(3), 724-728. DOI: 10.1016/j.cap.2009.06.060.

[26] Liqiang, J., Yichun, Q., Baiqi, W., Shudan, L., Baojiang, J., Libin, Y., Wei, F., Honggang, F., Jiazhong, S. (2006). Review of photoluminescence performance of nano-sized semiconductor materials and its relationships with photocatalytic activity. *Solar Energy Materials and Solar Cells*, 90(12), 1773-1787. DOI: 10.1016/j.solmat.2005.11.007.

[27] Tian, J., Li, J., Guo, Y., Liu, Z., Liu, B., Li, J. (2024). Oxygen vacancy mediated bismuth-based photocatalysts. *Advanced Powder Materials*, 3(4), 100201. DOI: 10.1016/j.apmate.2024.100201.

[28] Marschall, R. (2014). Semiconductor composites: strategies for enhancing charge carrier separation to improve photocatalytic activity. *Advanced Functional Materials*, 24(17), 2421-2440. DOI: 10.1002/adfm.201303214.

[29] Sharma, A., Tahir, M., Ahamad, T., Kumar, N., Sharma, S., Kumari, M., Khan, M.M., Takhur, S., Raizada, P. (2023). Improved charge transfer and enhanced visible light photocatalytic activity of Bi2O3@ Fe-MOF for degradation of Rhodamine B and Triclopyr. *Journal of King Saud University-Science*, 35(10), 102922. DOI: 10.1016/j.jksus.2023.102922.

[30] Dinesh, G.K., Saranya, R. (2024). Sonochemical facile synthesis of bismuth oxide nanoparticles using citrus lemon extract and its catalytic activity on azo dye degradation. *Water, Air, & Soil Pollution*, 235(10), 621. DOI: 10.1007/s11270-024-07364-4.

[31] Oudghiri-Hassani, H., Rakass, S., Al Wadaani, F.T., Al-Ghamdi, K.J., Omer, A., Messali, M., Abboudi, M. (2015). Synthesis, characterization and photocatalytic activity of α-Bi2O3 nanoparticles. *Journal of Taibah University for Science*, 9(4), 508-512. DOI: 10.1016/j.jtusci.2014.11.005.

[32] Malathy, P., Vignesh, K., Rajarajan, M., Suganthi, A. (2014). Enhanced photocatalytic performance of transition metal doped Bi2O3 nanoparticles under visible light irradiation. *Ceramics International*, 40(1), 101-107. DOI: 10.1016/j.ceramint.2013.06.032.

[33] Ali, N.D., Saed, U.A., Abdulnabi, W.A., Zeitoun, Z. (2026). Visible-Light Photocatalytic Degradation of Metronidazole Using Bismuth Oxide-Doped Erbium Oxide Anchored Graphene Oxide Nanocomposites: Kinetics and Mechanism. *Bulletin of Chemical Reaction Engineering & Catalysis*, 21(3), 553-568. DOI: 10.9767/bcrec.20651.

[34] Thanh, N.D., Thi, N.T., Nguyen, V.C., Le Pham, H.A. (2026). Facile Fabrication of Alginate–BiBDC Composite Beads for Efficient Removal of Methylene Blue from Aqueous Solutions. *Bulletin of Chemical Reaction Engineering & Catalysis*, 21(3), 539-552. DOI: 10.9767/bcrec.20680.

[35] Matinise, N., Botha, N., Fall, A., Maaza, M. (2025). Enhanced photocatalytic degradation of methylene blue using zinc vanadate nanomaterials with structural and electrochemical properties. *Scientific Reports*, 15(1), 26333. DOI: 10.1038/s41598-025-26333-0.

[36] Akpan, U.G., Hameed, B.H. (2009). Parameters affecting the photocatalytic degradation of dyes using TiO2-based photocatalysts: a review. *Journal of Hazardous Materials*, 170(2-3), 520-529. DOI: 10.1016/j.jhazmat.2009.05.039.

[37] Chen, Y.-W., Hsu, Y.-H. (2021). Effects of reaction temperature on the photocatalytic activity of TiO2 with Pd and Cu cocatalysts. *Catalysts*, 11(8), 966. DOI: 10.3390/catal11080966.

[38] Barakat, N.A., Kanjwal, M.A., Chronakis, I.S., Kim, H.Y. (2013). Influence of temperature on the photodegradation process using Ag-doped TiO2 nanostructures: negative impact with the nanofibers. *Journal of Molecular Catalysis A: Chemical*, 366, 333-340. DOI: 10.1016/j.molcata.2012.10.008.

[39] Ollis, D.F. (2018). Kinetics of photocatalyzed reactions: five lessons learned. *Frontiers in Chemistry*, 6, 378. DOI: 10.3389/fchem.2018.00378.

[40] Tran, H.D., Nguyen, D.Q., Do, P.T., Tran, U.N.P. (2023). Kinetics of photocatalytic degradation of organic compounds: a mini-review and new approach. *RSC Advances*, 13(25), 16915-16925. DOI: 10.1039/d3ra01970e.

[41] Fujishima, A., Zhang, X., Tryk, D.A. (2008). TiO2 photocatalysis and related surface phenomena. *Surface Science Reports*, 63(12), 515-582. DOI: 10.1016/j.surfrep.2008.10.001.

[42] Chen, X., Mao, S.S. (2007). Titanium dioxide nanomaterials: synthesis, properties, modifications, and applications. *Chemical Reviews*, 107(7), 2891-2959. DOI: 10.1021/cr0500535.

[43] Makama, A., Salmiaton, A., Choong, T., Hamid, M., Abdullah, N., Saion, E. (2020). Influence of parameters and radical scavengers on the visible-light-induced degradation of ciprofloxacin in ZnO/SnS2 nanocomposite suspension: Identification of transformation products. *Chemosphere*, 253, 126689. DOI: 10.1016/j.chemosphere.2020.126689.

[44] Low, J., Cheng, B., Yu, J. (2017). Surface modification and enhanced photocatalytic CO2 reduction performance of TiO2: a review. *Applied Surface Science*, 392, 658-686. DOI: 10.1016/j.apsusc.2016.09.093.

[45] Nosaka, Y., Nosaka, A.Y. (2017). Generation and detection of reactive oxygen species in photocatalysis. *Chemical Reviews*, 117(17), 11302-11336. DOI: 10.1021/acs.chemrev.7b00161.

[46] Sun, W., Zhang, H., Lin, J. (2014). Surface modification of Bi2O3 with Fe (III) clusters toward efficient photocatalysis in a broader visible light region: implications of the interfacial charge transfer. *The Journal of Physical Chemistry C*, 118(31), 17626-17632. DOI: 10.1021/jp503845g.